Precipitation Features Observed by Doppler Radar at Tuktoyaktuk, Northwest Territories, Canada, during the Beaufort and Arctic Storms Experiment

YOSHIO ASUMA, SOSHI IWATA, AND KATSUHIRO KIKUCHI

Division of Earth and Planetary Sciences, Graduate School of Science, Hokkaido University, Sapporo, Japan

G. W. KENT MOORE

Department of Physics, University of Toronto, Toronto, Ontario, Canada

RYUJI KIMURA AND KAZUHISA TSUBOKI

Ocean Research Institute, University of Tokyo, Tokyo, Japan

(Manuscript received 5 February, in final form 21 November 1997)

ABSTRACT

In the fall of 1994, the Beaufort and Arctic Storms Experiment (BASE) was held to collect information on the structure and evolution of mesoscale weather systems over the southern Beaufort Sea and the Mackenzie River delta of the western Canadian Arctic. As part of the experiment, X-band Doppler radar observations were carried out at Tuktoyaktuk, a village on the shore of the Beaufort Sea. In this paper, the precipitation features, structure, and moisture transport associated with two distinctly different weather systems that were observed during BASE are described with a variety of datasets. Climatologies of storm activity in the area suggest these two types of different weather systems, the so-called Pacific origin and storm track disturbances, are the most frequently observed in this region during the fall months.

The characteristic feature of a Pacific origin weather system is a pronounced layering of the air masses. In the upper layer, the air mass is of Pacific origin and is associated with a deep low in the Gulf of Alaska. As a result it is moist and is capable of producing precipitation. In contrast, the lower layer is initially of continental origin and is associated with a secondary lee cyclogenesis event in the Mackenzie River basin. As the secondary disturbance moves to the east, there is a shift in the wind direction that advects air from the Beaufort Sea into the lower layer. This results in a moistening of the lower layer that allows precipitation from the upper layer that had previously evaporated in the lower layer to be enhanced and reach the surface. The detailed structure of this type of storm is strongly affected by the topography of the region and the presence of open water in the southern Beaufort Sea.

The storm track weather system is markedly different and is associated with the passage of a mesoscale low over the southern Beaufort Sea. In this sort of system, there is a well-defined frontal structure of a type previously identified in the midlatitudes. Two different precipitation regimes are identified that are associated with the passage of the warm and cold front. In this sort of system, the sources of moisture are the Bering Sea and the open water in the southern Beaufort Sea.

1. Introduction

The first intensive meteorological research observations in the western Canadian Arctic were conducted by a Japanese cloud physics research group in the winter of 1977 at Inuvik, Northwest Territories, Canada. These observations were continued for several years during the winter season (Magono 1978; Kikuchi and Kajikawa 1979; Magono and Kikuchi 1980; Higuchi et al. 1981; Takeda et al. 1982; Kikuchi et al. 1982; Fujiyoshi et al. 1982; Kikuchi 1987). The research that was carried out focused on understanding the physical processes responsible for the formation of the snow crystals that formed in the very cold temperatures typical of the region during the winter. Kikuchi and Kajikawa (1979) reported the existence of peculiar shapes of snow crystals that had previously been observed in Antarctica (Kikuchi 1970). Magono and Kikuchi (1980) reported that the crystals formed in the temperatures as warm as $-10°C$ or $-15°C$ but were observed at surface temperatures as cold as $-30°C$ or $-40°C$. These low temperatures inhabited rapid crystals growth, and as a result it was concluded that the crystal formed aloft in warmer

Corresponding author address: Yoshio Asuma, Division of Earth and Planetary Sciences, Graduate School of Science, Hokkaido University, Kita 10 Nishi 8, Kita-ku, Sapporo 060-0810, Japan.
E-mail: asuma@geophys.hokudai.ac.jp

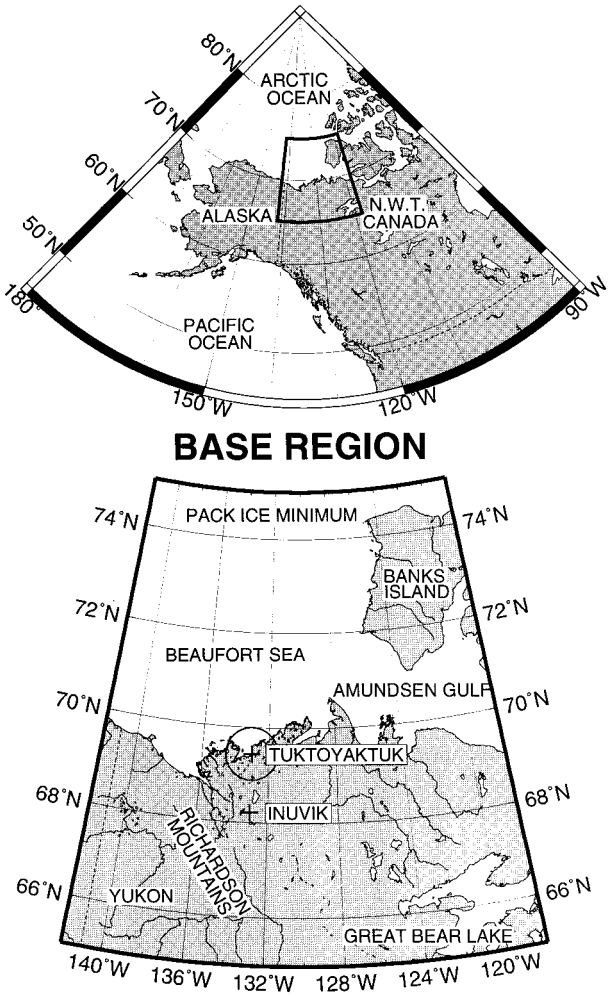

FIG. 1. Maps for BASE experimental region. The experimental region is shown in the thick sector in the upper figure. The lower figure shows an enlarged map of the BASE region. An X-band Doppler radar was set up at Tuktoyaktuk. A circle at Tuktoyaktuk shows the detectable range (60 km) of the radar.

and moister air of Pacific origin. Takeda et al. (1982) discussed the temperature profiles in the clouds associated with the synoptic conditions at Inuvik in midwinter. Kikuchi et al. (1982) and Fujiyoshi et al. (1982) further investigated crystal habits and their formation processes using X-band and Ka-band radar systems. They reported on the environment in which the precipitation processes occurred but, due to a lack of enhanced mesoscale and synoptic scale observation, were unable to document the larger-scale environment in which the precipitation was embedded. In addition, their observations were restricted to the winter season when precipitation is relatively light.

Hudak et al. (1995) reported on the synoptic conditions over the southern Beaufort Sea and the Mackenzie River delta. They reported that the fall was the period during the year when the storm frequency was highest. In particular, they showed that the storm frequency increased from early August until mid-October and then rapidly decreased in late October and early November. They surmised that this distribution was the result of the larger-scale circulation pattern over the region and the energy exchange between the atmosphere and the Beaufort Sea that is possible when the latter is ice free. The rapid reduction in storm frequency late in the fall was hypothesized to be the result of the freezing over of the Beaufort Sea.

The Beaufort and Arctic Storms Experiment (BASE) project was carried out over the southern Beaufort Sea and Mackenzie River delta during the fall of 1994. The purpose of the project was to improve the prediction of weather systems in the region and to improve our understanding of the role that these weather systems have on the climate of the western Arctic.

In addition to improving our understanding of weather systems in the region, BASE also addressed the implications that these systems have on the climate of the region. The impact of cloud systems and their micro- and mesoscale processes on the climate is one of the issues that is being addressed by the Global Energy and Water Cycle Experiment (GEWEX) (Chanine 1992; Ryan 1996). The discharge from the north-flowing rivers that drain into the Arctic Ocean is important: in maintaining the pycnocline in the Arctic Ocean (Barry et al. 1993), in regulating sea ice production (Cattle 1985), and in regulating deep oceanic convection in the Nordic Sea (Aggaard and Carmack 1989). It follows that the weather systems that produce precipitation in these basins are an important component of the global climate system. In recognition of this, the Mackenzie River basin has been selected as the site for one of the fine regional experiments under the GEWEX Hydrometeorological Panel. The weather systems described in this paper and in particular the factors that control the production of precipitation are therefore of interest to GEWEX.

2. Observations and analyzed dataset

The BASE experimental region was located over the southern Beaufort Sea including Banks Island and the Mackenzie delta in the northern Yukon Territory and the northwest part of the Northwest Territories in the Canadian Arctic. This region is adjacent to Alaska in the United States. A map of the region is shown in Fig. 1.

The BASE experimental region is situated between the mountainous region of the west coast of the North American continent and the central plateau region of the Canadian Shield. The Richardson Mountains, with an elevation exceeding 1000 m, extend along the southwestern part of the region. A flat low-level plateau extends eastward with the Mackenzie River along its western edge. The delta is a maze of meandering small channels. Uncountable lakes, swamps, and marshes are spread over the plateau and delta as a result of the poor

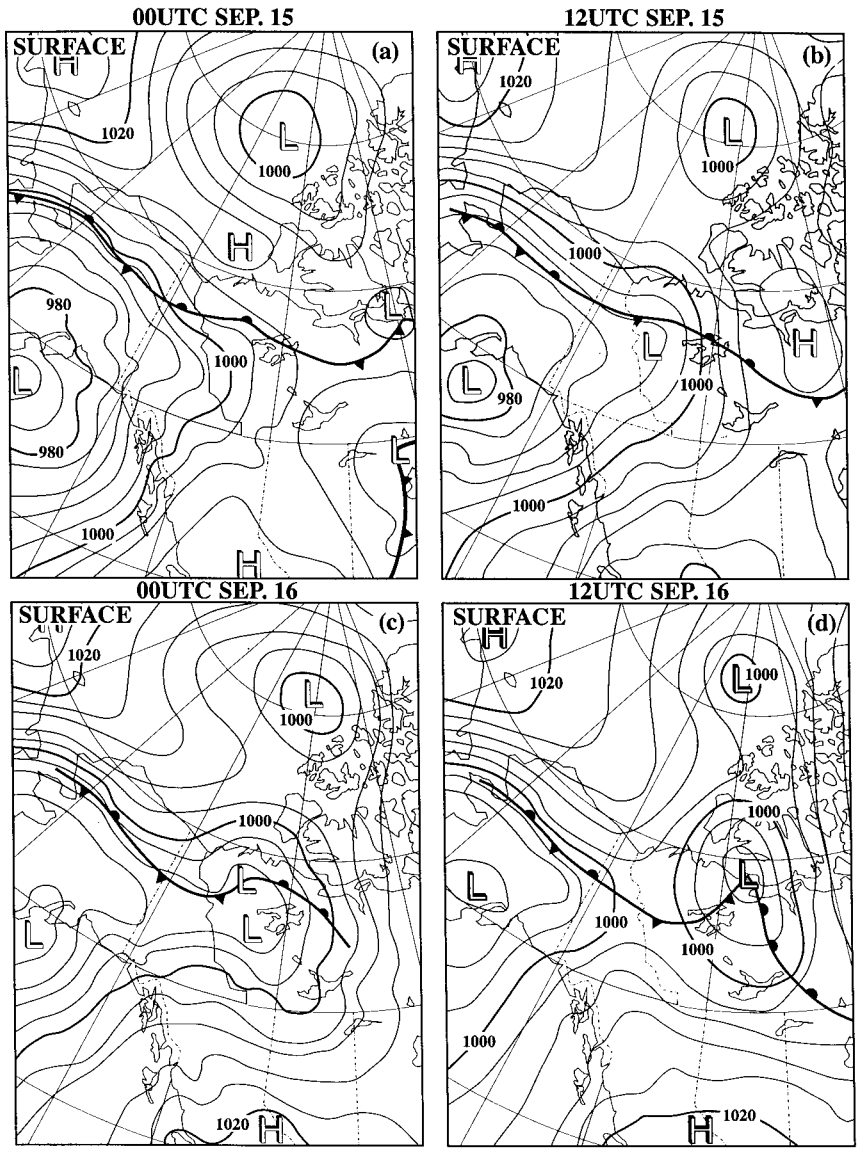

FIG. 2. Surface synoptic charts for a Pacific origin disturbance (IOP-04). Charts at (a) 0000 UTC and (b) 1200 UTC 15 September 1994: (c) 0000 UTC and (d) 1200 UTC 16 September 1994.

drainage over the underlying permafrost. The Beaufort Sea is situated to the north of the BASE region. August is the period of the year when the ice pack is at its minimum. As the period of the experiment progressed, the extent of sea ice gradually increased. However, throughout the period there was open water present off Tuktoyaktuk.

The BASE project was organized by the Atmospheric Environment Service (AES) of Canada and the University of Toronto. Other foreign organizations, including Hokkaido University of Japan, the National Center for Atmospheric Research (NCAR), and the Central Aerological Observatory of Russia, also participated in the project. BASE was mainly conducted out of Inuvik and Tuktoyaktuk. The main research assets were two aircraft [Convair 580 of the National Research Council of Canada, and C-130 of NCAR] and two X-band Doppler radar systems (Hokkaido University and University of Toronto). The X-band dual-polarization Doppler radar (wavelength: 3.2 cm, peak power: 40 kW, antenna diameter: 1.2 m) on the seashore of Beaufort Sea at Tuktoyaktuk was set up by Hokkaido University. Plan position indicator (PPI) data of reflectivity and Doppler velocity at four different elevation angles (1°, 3°, 5°, and 10°) were collected every 10 min. Mesonet stations were set up at radar sites by Hokkaido University and

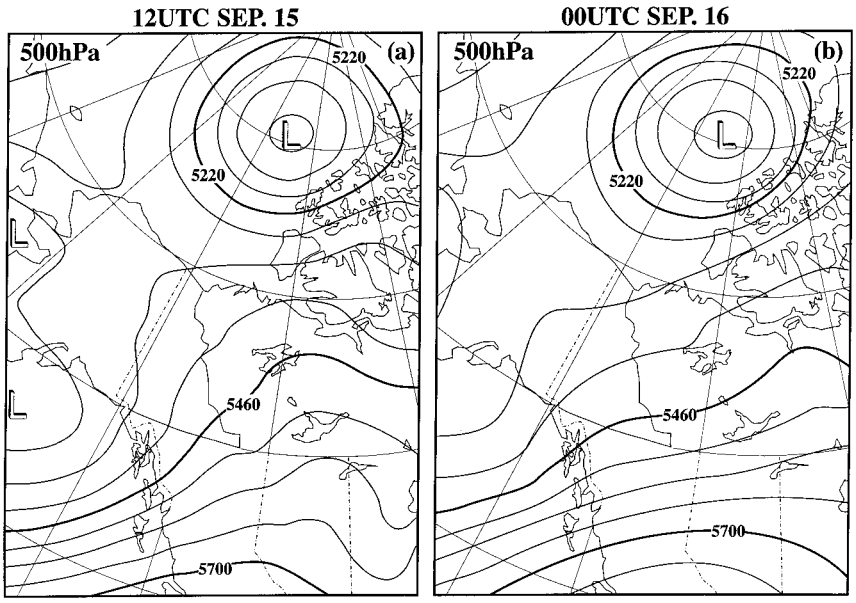

FIG. 3. 500-hPa charts at (a) 1200 UTC 15 September and (b) 0000 UTC 16 September 1994.

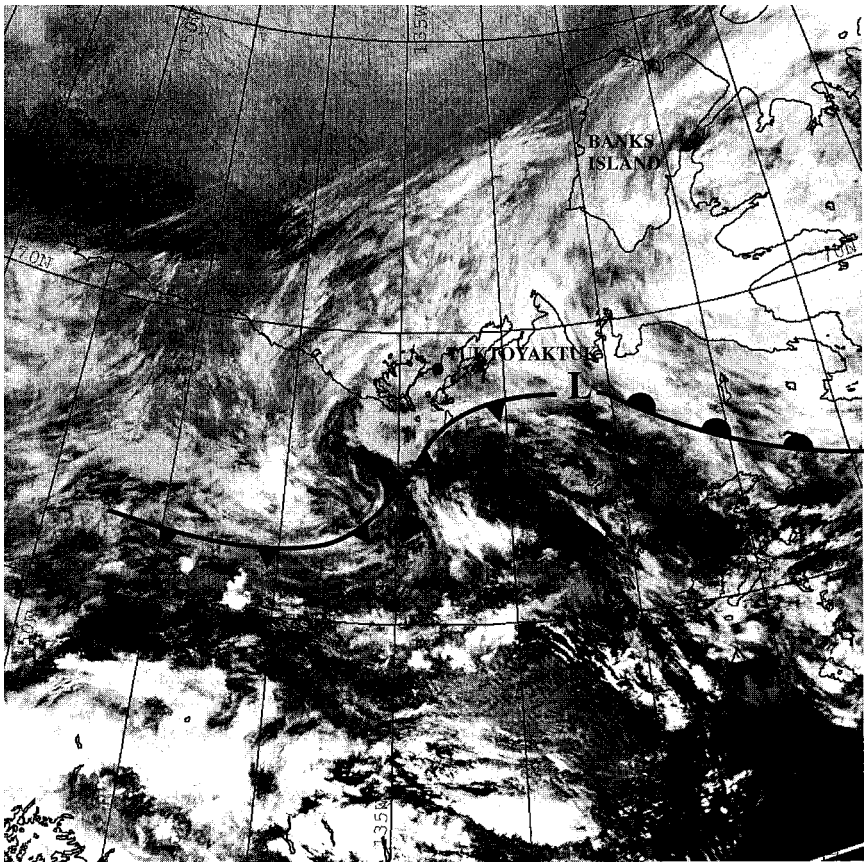

FIG. 4. NOAA AVHRR channel image of 0449 UTC 16 September 1994. The locations of the secondary lee cyclone labeled L; warm and cold fronts were superimposed on the image.

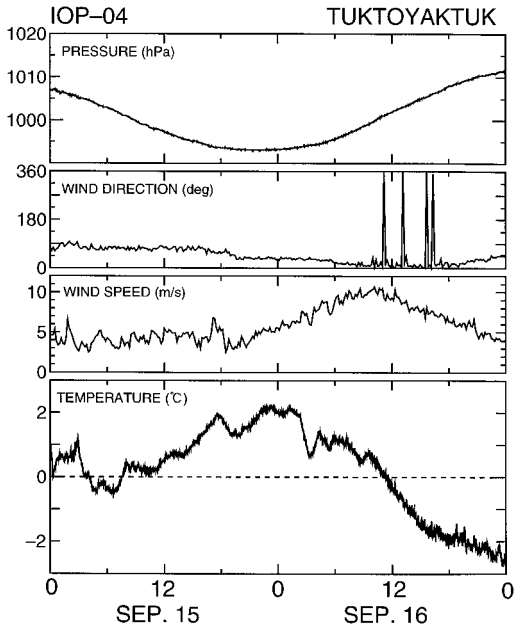

FIG. 5. Time variations of the surface pressure, winds, and temperature recorded at the radar site during IOP-04.

AES. Intensive upper-air observations were also conducted by AES at Tuktoyaktuk, Inuvik, Norman Wells, and Whitehorse. Satellite images were received by the University of Toronto at Inuvik. The objectively analyzed dataset (GANAL) used in this paper was provided by the Japan Meteorological Agency (JMA).

3. Storm categories

There were 13 intensive observational periods (IOPs) during BASE. The disturbances observed can be classified into four of the storm types discussed by Hudak et al. (1995). There were four disturbances of the ''Pacific origin'' type, seven of the ''storm track'' type, and one each of the ''Arctic highs'' and ''cold lows'' types. According to the Hudak et al. climatological study, the most frequent disturbances in September are the Pacific origin types. In October, the frequencies of the storm track and Arctic highs types increase and that of the Pacific origin decrease. During BASE, approximately 80% of disturbances were of the Pacific origin or storm track type. Compared with the climatological data, the Pacific origin type was less common and the storm track more common during the BASE. However, when added together they accounted for approximately 80% of the storm systems observed during BASE. This frequency

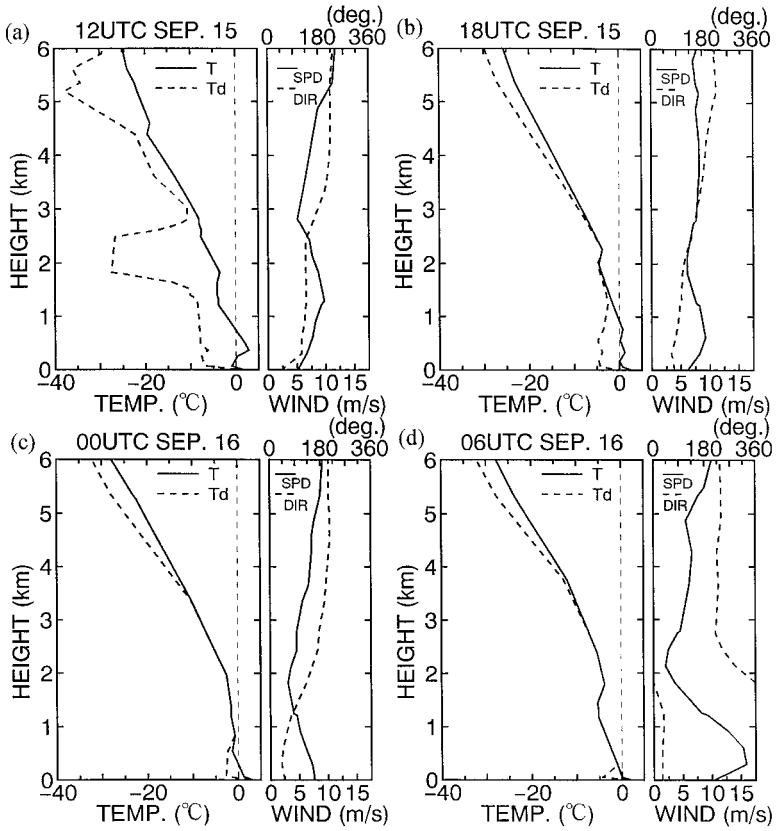

FIG. 6. Upper-air soundings taken at Tuktoyaktuk: (a) 1200 UTC and (b) 1800 UTC 15 September 1994, and (c) 0000 UTC and (d) 0600 UTC 16 September 1994.

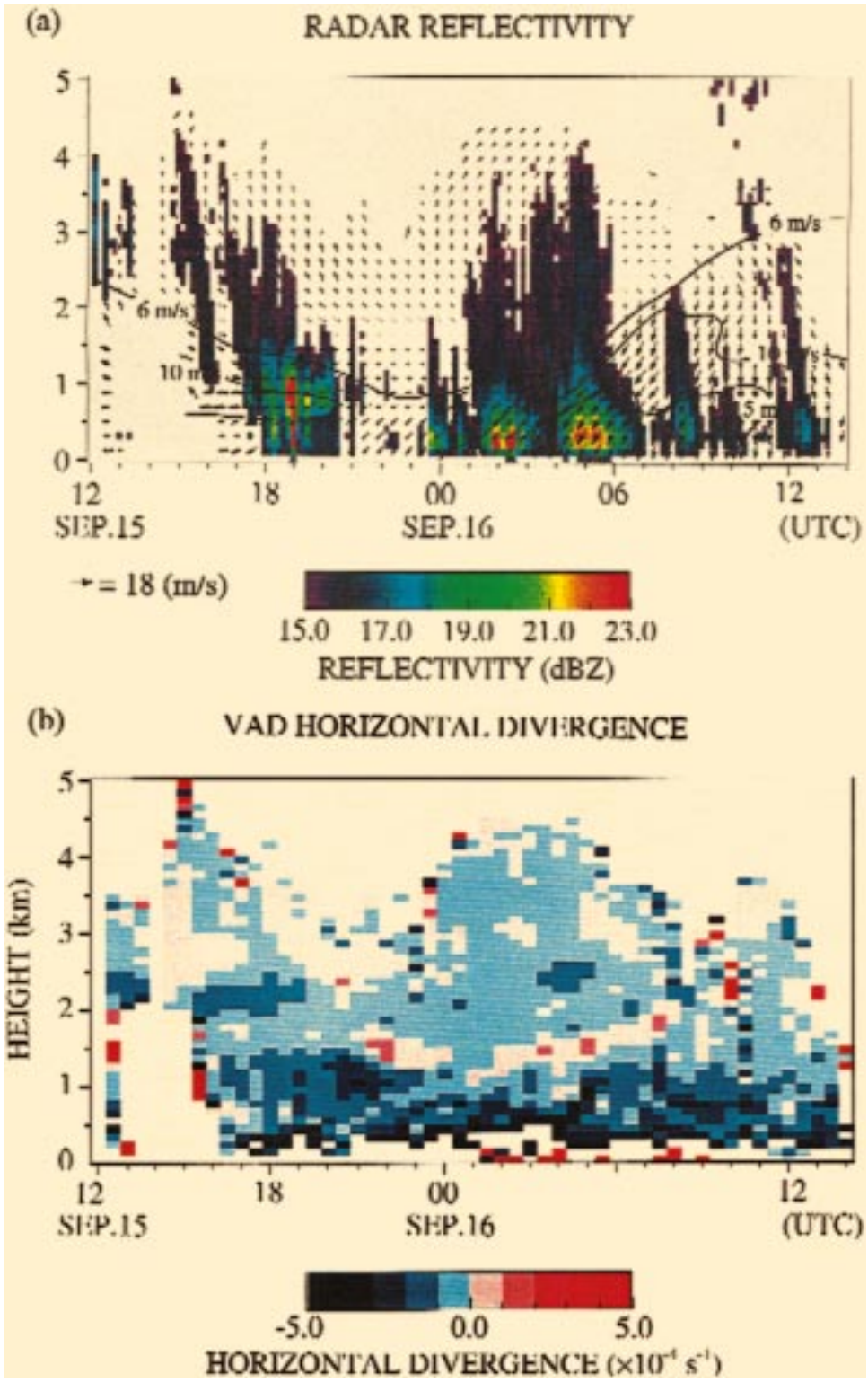

FIG. 7. Time–height variations of (a) radar reflectivity, horizontal winds, and (b) horizontal divergence during IOP-04.

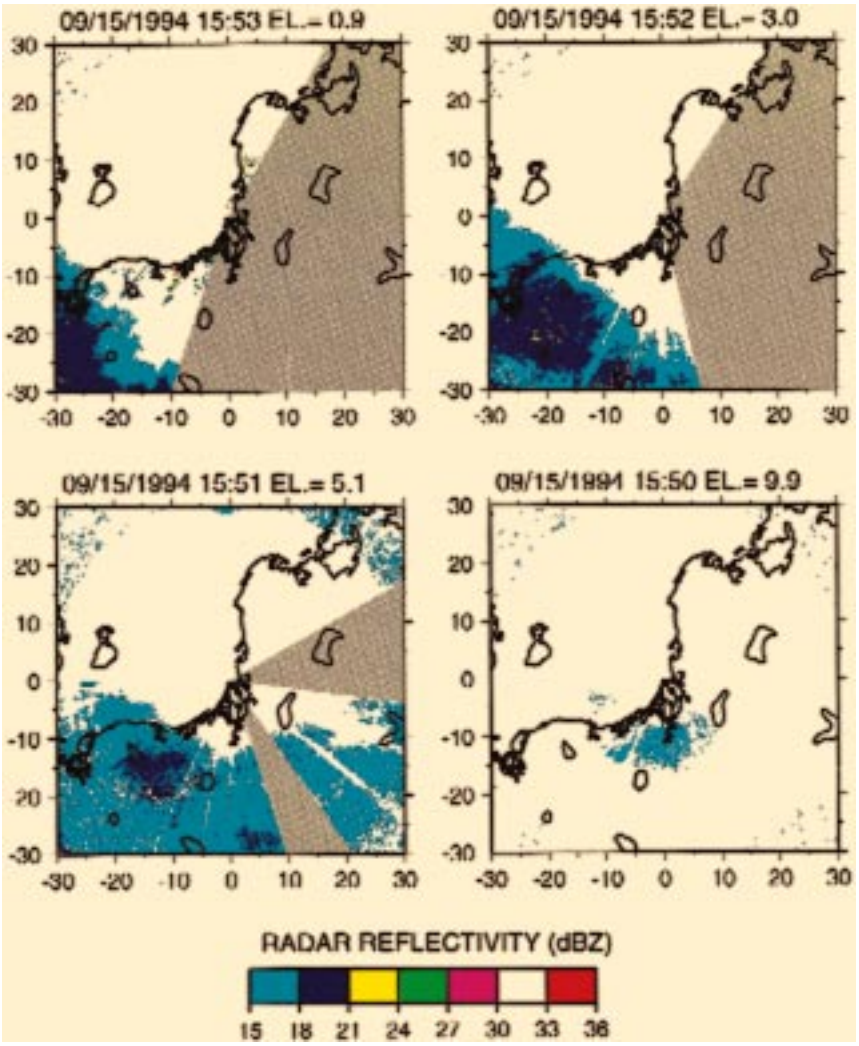

FIG. 8. Snapshots of PPI radar echoes at four different elevation angles for the early stage.

is almost the same one as that for the climatology. As a result of the dominance of these two systems, this paper will focus on discussing the features associated with a typical example of each of them.

4. A Pacific origin disturbance

a. Synoptic conditions

The Pacific origin disturbance that we will focus on was observed from 1800 UTC 14 September 1994 to 1200 UTC 16 September 1994 (BASE IOP-04). Representative surface synoptic charts for this period are shown in Fig. 2. One can see that during the IOP, stationary and deep lows were situated over the Gulf of Alaska and the northern Beaufort Sea. An Arctic front was analyzed between these two lows. The interaction of the Gulf of Alaska low with topography to the west of the Mackenzie Basin resulted in the development of a lee cyclone around 0000 UTC on the 15th. The secondary low that resulted moved rapidly eastward and deepened as it interacted with the stationary Arctic front. The low was located to the south of the Tuktoyaktuk radar site around 0000 UTC on the 16th.

This secondary low was a very shallow disturbance. This can be seen from the 500-hPa charts shown in Fig. 3. One can clearly identify the two major low pressure systems. However, there is little evidence of the secondary lee low cyclone that was spawned from the Gulf of Alaska low.

A National Oceanic and Atmospheric Administration (NOAA) Advanced Very High Resolution Radiometer (AVHRR) channel 4 infrared image from 0449 UTC on the 16th is shown in Fig. 4. At this time, the secondary low, labeled L, was to the east of Tuktoyaktuk. From this image, one can recognize the distinct Arctic front that extends outward from the center of the depression

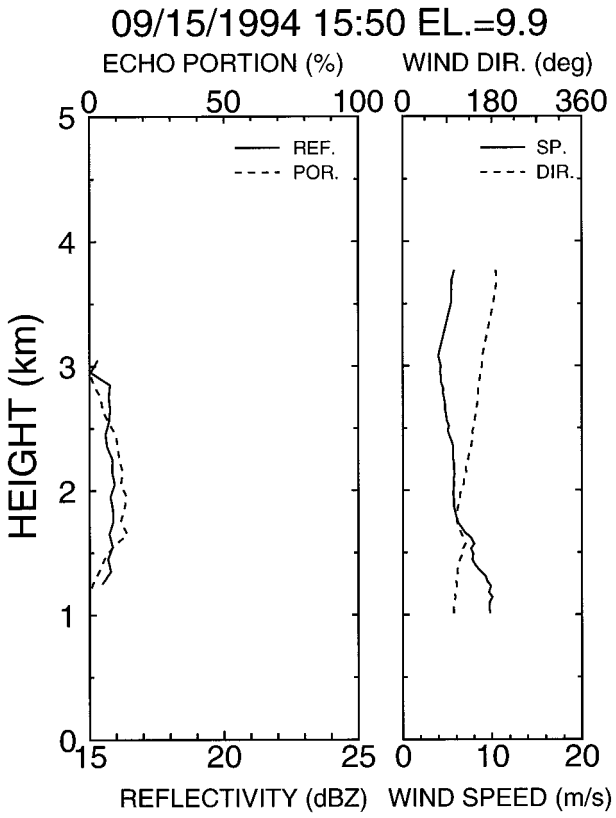

FIG. 9. Vertical profiles of reflectivity, echo portion, and wind calculated from 10° PPI data.

as well as the low-level stratus clouds over the open water of the Beaufort Sea.

Figure 5 shows the time variation of the surface pressure, winds, and temperature as recorded by the automatic weather station collocated with the radar. The minimum pressure of 993 hPa was recorded at 2200 UTC on the 15th. Prior to this time, the winds were light, with a magnitude of approximately 4 m s^{-1}, and were from the east. Afterward, the winds intensified in strength, with a magnitude of approximately 10 m s^{-1}, and were from the north. The surface air temperature gradually increased prior to the time of minimum pressure and decreased rapidly afterward.

Soundings taken at Tuktoyaktuk made every 6 h from 1200 UTC on the 15th to 1200 UTC on the 16th are shown in Fig. 6. A strong layering is evident in the 1200 UTC sounding on the 15th. One can clearly see a moist upper-level layer associated with a southwesterly flow between 2.5 and 4.3 km mean sea level (MSL). Below 2.3 km MSL, the air was dry and the wind was from the east. The peak wind speed of approximately 10 m s^{-1} occurred at the 1.2 km MSL level. Over the next 24 h, there was a pronounced moistening of the lower layer as the wind direction shifted so that the wind was from the north. This was associated with an increase in the strength of the winds below 1 km. Above 2 km MSL, there was no change in the properties of the upper air mass. At 1800 UTC on the 15th, one can see that an isothermal layer near 0°C existed between the surface and approximately 1 km MSL. Afterward, the melting level (0°C level) rapidly approached the surface.

b. Radar observations

The time–height variation of radar reflectivity, the horizontal wind field, and its divergence are shown in Fig. 7. The radar reflectivity was averaged every 10 min using PPI data stronger than 15 dBZ at a 10° elevation angle. The horizontal wind field and its divergence were calculated with the velocity azimuth display (VAD) method of Browning and Wexler (1968). Snapshots of PPI radar echoes in four different elevation angles (1°, 3°, 5°, and 10°) are shown in Figs. 8 and 10. Vertical profiles of the reflectivity, the echo portion, and wind field using 10° PPI data are indicated in Figs. 9 and 11. The echo portion is defined as the percentage of area that has stronger reflectivity than 15 dBZ in 10° PPI data.

A weak radar echo appeared in the layer between 2 and 4 km MSL at 1200 UTC on the 15th. The precipitation in this layer at this time did not reach the ground. An example of radar echo in the early stage and vertical profile are shown in Figs. 8 and 9. A weak layered echo was approaching from the south between 1 and 3 km MSL. The easterly with magnitude approximately 10 m s^{-1} was analyzed below 1.5 km MSL. Above 1.5 km MSL, the lighter wind shifted its direction from the southeasterly to the southerly with height. Over the next 24 h, precipitation was present below 4 km MSL. The precipitation appeared to be organized into cells that occurred every 3 h. The precipitation reached the ground. When the cell approached, radar echoes were extended to the higher altitude and enhanced in the lower layer. An example is shown in Figs. 10 and 11. Monotonous layered echoes were observed. Radar echo in 1° elevation angle seemed to be enhanced by the melting. The vertical profile in Fig. 11 shows the radar echo appeared below 2.7 km MSL. Weaker radar echo in the upper layer, gradually increased below 1.3 km MSL and the strongest reflectivity was recognized near the ground. A stronger northeasterly was analyzed below 1.3 km MSL and weaker southerly above this level. Partially melted larger wet snowflakes were observed by the precipitation video camera set up at the radar site. The surface air temperature was about 2.0°C at 0000 UTC on the 16th, as shown in Fig. 5. The melting level was observed at 300 m MSL and it rapidly decreased 60 m MSL at 0600 UTC by upper-air sounding (as shown in Fig. 6). As the precipitation particles were partially melted near the ground, radar echoes with 1° elevation angle were identified to be in the ''bright band.'' But it is clear from Fig. 7 that the precipitation enhancement occurred below 1.3 km MSL. This altitude is higher than the melting layer. The precipitation par-

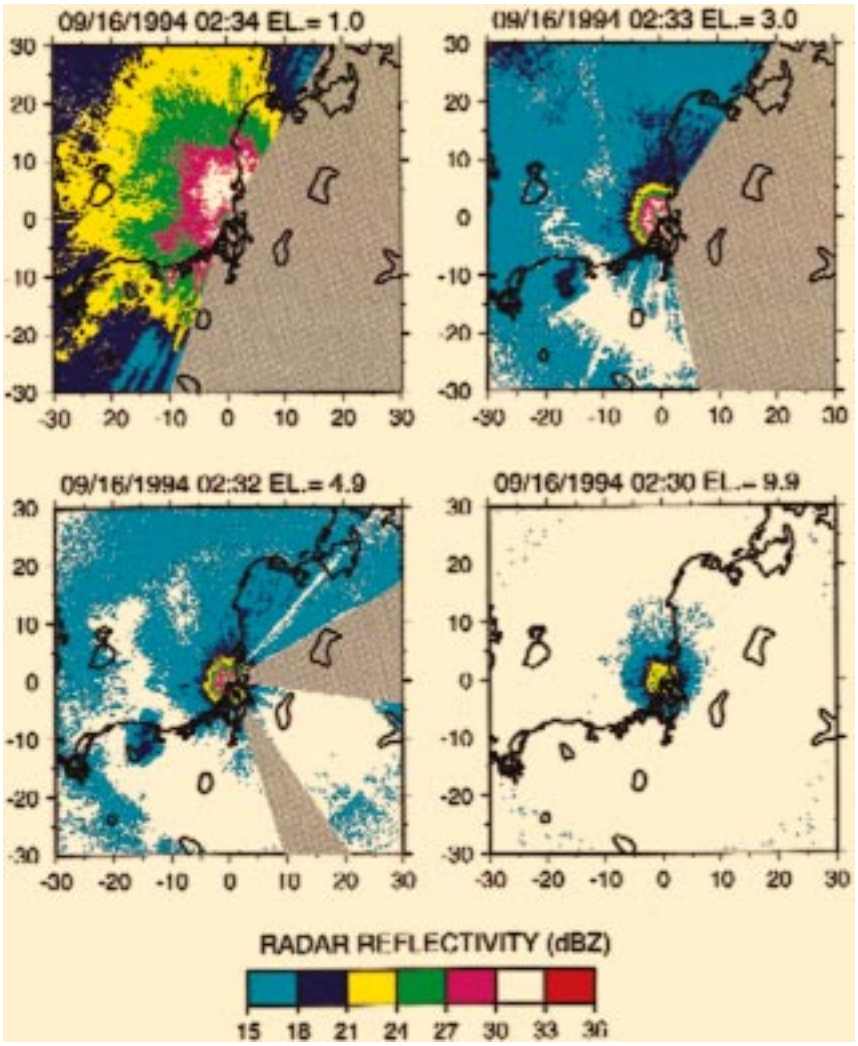

FIG. 10. Same as Fig. 8 but for second stage.

ticles became larger snowflakes collecting small ice crystals and small droplets and aggregated in the lower layer below 1.3 km MSL.

The horizontal wind field derived from the radar data shown in Fig. 7a is consistent with the soundings displayed in Fig. 6. Two distinct layers can be recognized. Continuous and relatively weak, wind speeds less than 6 m s^{-1} were observed in the upper layer above 2 km MSL. The wind speed was generally higher, in excess of 10 m s^{-1}, in the surface layer. As discussed previously, there was a shift in wind direction from easterly to northerly, and an increase in wind speed occurred between 1800 UTC on the 15th and 1200 UTC on the 16th. This was associated with the passage of the secondary low evident in Figs. 5 and 6.

The radar-derived horizontal wind divergence field shown in Fig. 7b shows stronger and relatively uniform convergence in the layer below 1 km MSL. In contrast, a convergence in the upper layer was generally weaker and it was associated with the production of the precipitation. And weaker divergence appeared around it.

This structure is suggestive of the presence of ''generating cells'' in the upper layer (Gunn et al. 1954; Hobbs 1978). The fate of the precipitation produced in these cells was influenced by the conditions into which it fell. While the secondary depression was to the east of Tuktoyaktuk and one had easterly flow at the surface bringing relatively dry and warm air into the region, the precipitation generated aloft evaporated before hitting the ground. This acted to moisten the surface layer and ultimately allowed precipitation to reach the ground. This can be seen in the gradual lowering of the region in which radar echoes were observed from 1200 to 2200 UTC on the 15th. The change in wind direction that occurred around 0000 UTC on the 16th brought with it warm and relatively moist air from the Beaufort Sea. The precipitation from the upper layer was enhanced through aggregation of snow crystals and collection of

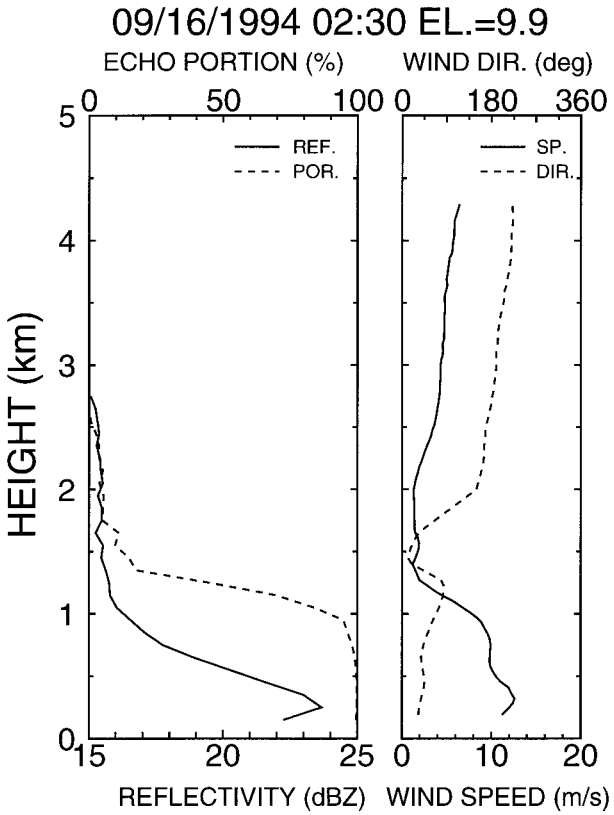

FIG. 11. Same as Fig. 9 but for 0230 UTC 16 September.

cloud droplets. And the melting was processed near the ground. This resulted in the high reflectivity that can be seen in Fig. 7a after 0000 UTC on the 16th.

c. Moisture transport

To investigate the horizontal transport of water vapor associated with this event, the upper-air soundings from Whitehorse, Norman Wells, Inuvik, and Point Barrow taken at 0000 UTC on the 15th and 16th are shown in Fig. 12. For reference, the surface pressure fields from Fig. 2 at these times are also shown. The presence of the synoptic low over the Gulf of Alaska resulted in southerly winds and low dewpoint depressions at Whitehorse, which is on the windward side of the Rocky Mountains. As the moist Pacific air mass moved northeastward, the mountains acted as a barrier allowing only the upper-level air to pass into the region. One can see evidence of this in the thin and saturated layers present at 0000 UTC on the 15th around 4 km MSL at Norman Wells and around 3.5 km MSL at Inuvik. In contrast, the entire lower atmosphere was dry at Point Barrow at this time. One day later at 0000 UTC on the 16th, the movement of the secondary low resulted in the moistening of the entire atmosphere below 3 km MSL at Inuvik. This is contrasted with the relatively dry conditions below 3 km MSL that were present at Norman Wells.

A more complete picture of the moisture transport is provided by making use of the meteorological fields provided by GANAL as carried out by JMA. The vapor flux (Q) is defined by

$$Q = qV,$$

where q is water vapor mixing ratio and V is horizontal wind on a given pressure surface. The vapor flux at the surface and the 700-hPa level, as derived from the JMA analyses, valid at 1200 UTC on the 15th and 0000 UTC on the 16th are shown in Fig. 13. Also shown are the mean sea level pressure and 700-hPa geopotential fields. At each time and level, both a synoptic scale as well as a mesoscale view centered on the BASE region are provided.

At the surface one can clearly see the convergence in moisture transport that occurs on the Pacific side of the barrier. In contrast at 700 hPa, moisture is flooding into the Mackenzie River basin. This is a clear bifurcation in the upper-level transport with a branch continuing eastward and a branch intruding northward into the BASE region. In the mesoscale view, the layered structure described previously is evident. At the surface, there is easterly flow bringing dry continental air into the area around Tuktoyaktuk. In contrast, there is southerly flow of moist air at 700 hPa. At 0000 UTC on the 16th, one can see the significant moistening at the surface that is the result of the northerly flow associated secondary low. At 700 hPa, the northerly branch of moist air has moved eastward but moist air mass was still supplied to the BASE region from the Pacific.

5. A "storm track" disturbance

a. Synoptic conditions

The disturbance of this type that will be discussed was observed from 1200 UTC 30 September to 1200 UTC 1 October 1994 (BASE IOP-10). Surface and 500-hPa charts for this period are shown in Fig. 14. During this event, a deep synoptic-scale low was located approximately 1000 km south of the Aleutian Islands (not shown in Fig. 14). A mesoscale low over the southern Beaufort Sea had developed earlier on the 28th and was propagating eastward along the ice edge (Renfrew and Moore 1996). As is typical of many high-latitude systems, the horizontal scale of this low was much smaller than that of midlatitude systems. This feature was quite deep and can clearly be seen on the 500-hPa surface charts. The low had well-defined warm and cold fronts as indicated in Fig. 14. The warm front associated with this low passed by Tuktoyaktuk around 1800 UTC 30 September, whereas the cold frontal passage occurred approximately 6 h later.

A NOAA AVHRR channel 4 satellite image at 1901 UTC 30 September is shown in Fig. 15. One can clearly

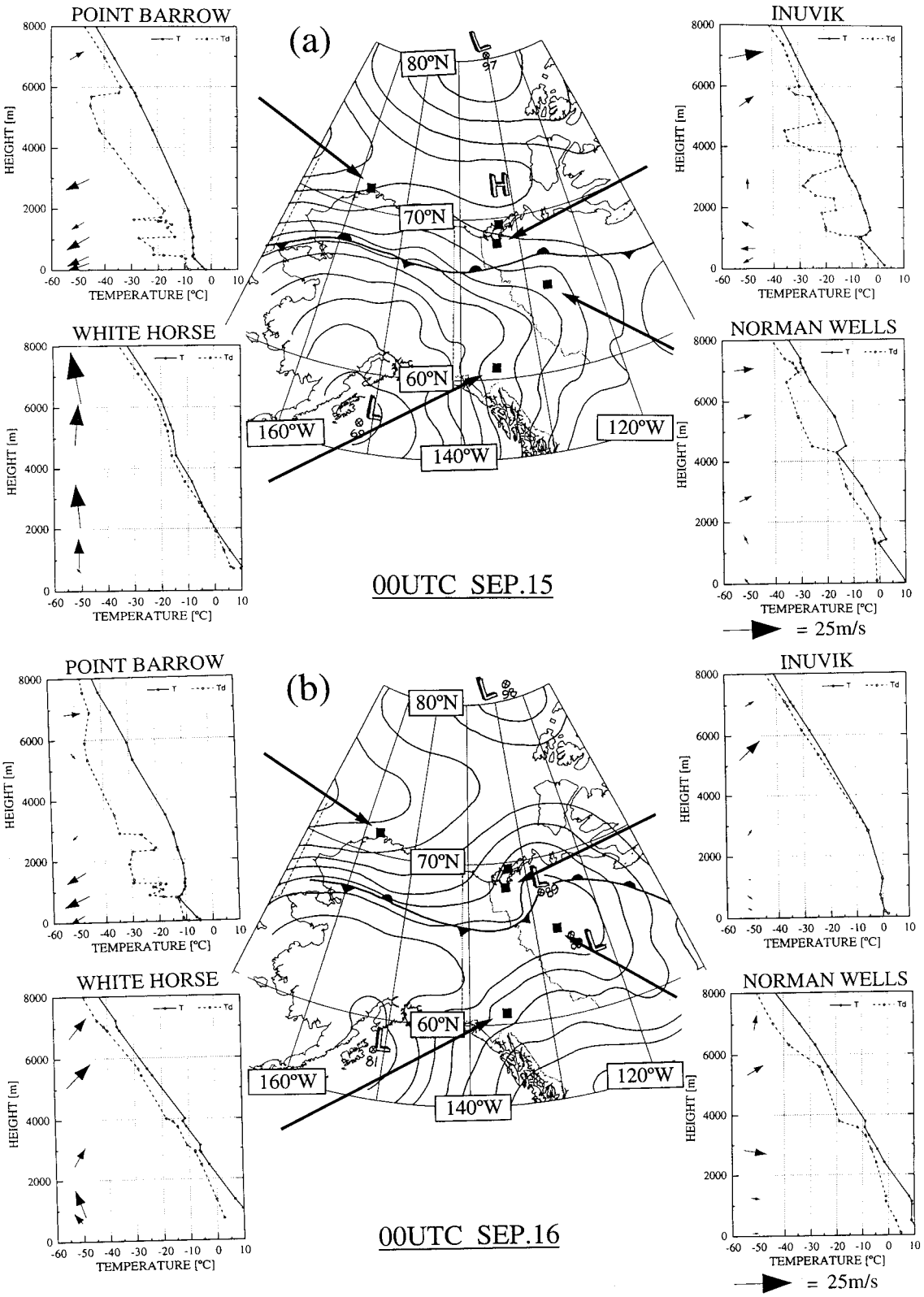

FIG. 12. Upper-air soundings at Whitehorse, Norman Wells, Inuvik, and Point Barrow taken at (a) 0000 UTC 15 September and (b) 0000 UTC 16 September 1994. The surface pressure fields are superimposed on the maps.

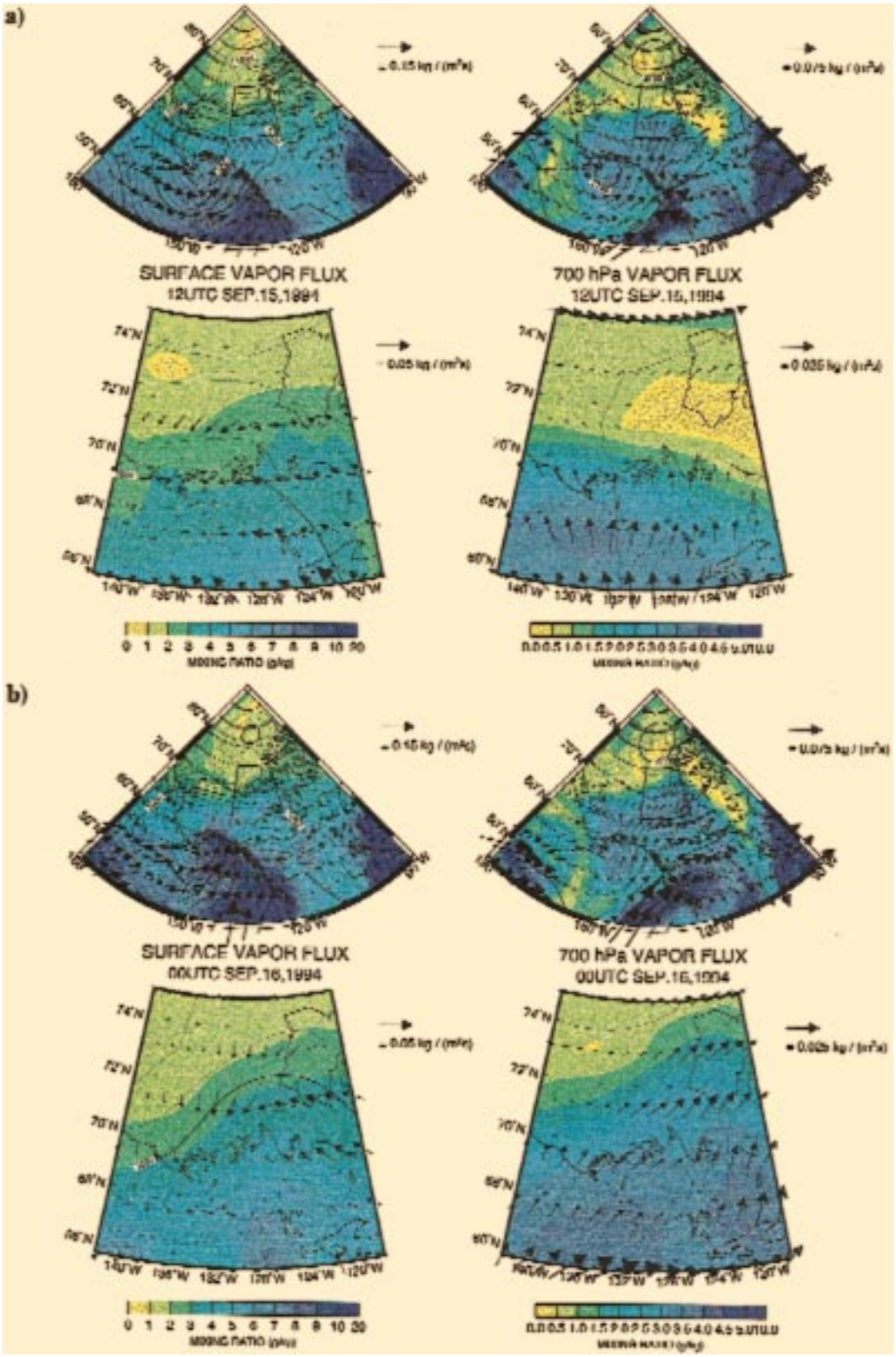

FIG. 13. The vapor flux (arrows), mixing ratio (shade), and the pressure (contour lines) at the surface and 700-hPa levels diagnosed from the GANAL analysis at (a) 1200 UTC 15 September and (b) 0000 UTC 16 September 1994.

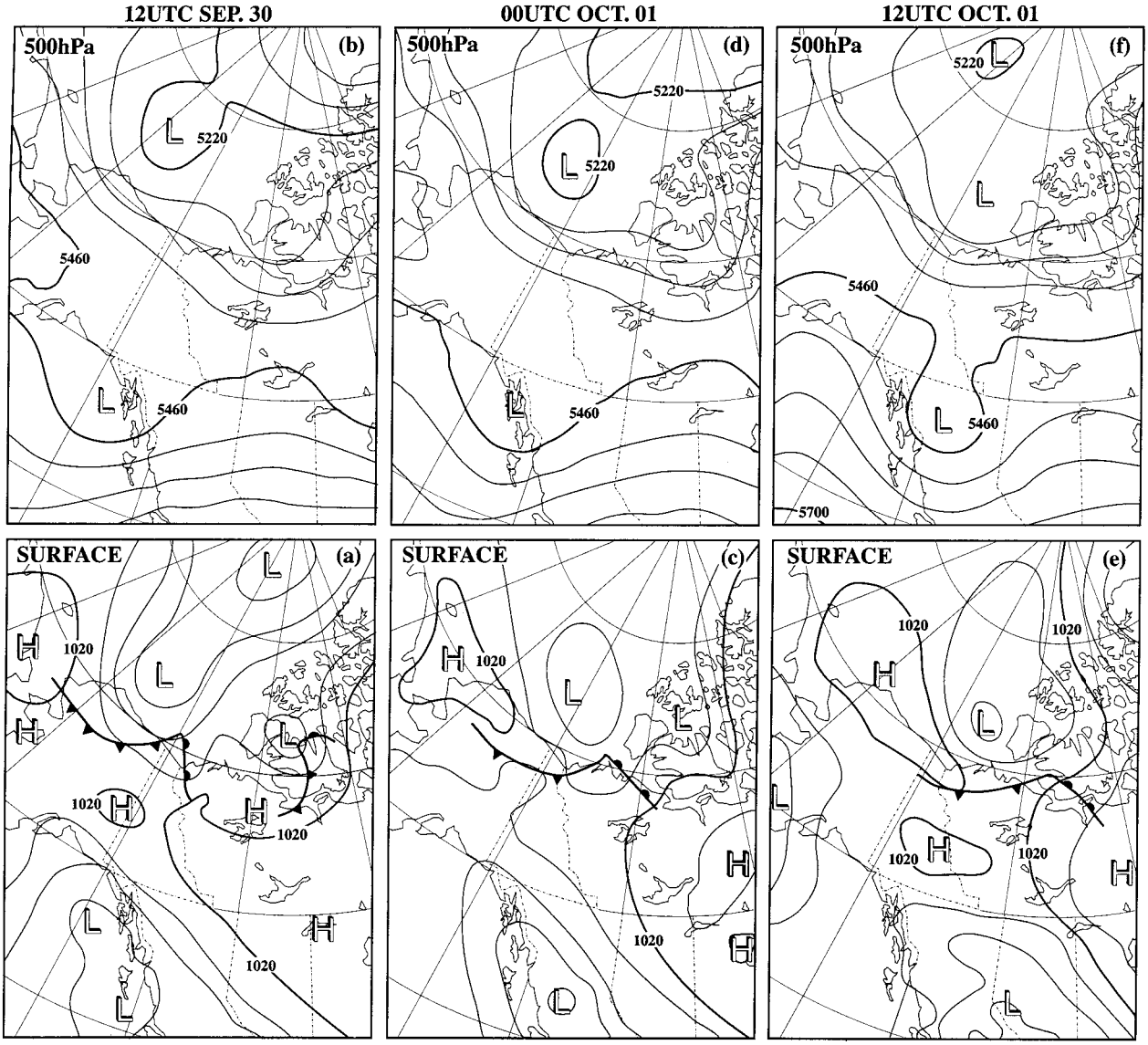

FIG. 14. Surface and 500-hPa synoptic charts for storm track disturbance (IOP-10) at (a) and (b) 1200 UTC 30 September, (c) and (d) 0000 UTC, and (e) and (f) 1200 UTC 1 October 1994.

see the vortex center near 73°N and 148°W, labeled L in the figure. The cold front can be seen extending along the coast line of Alaska and the Yukon. The warm front can also be recognized extending eastward from the low center. The image shows that the cloud heights along the cold front were lower over the land than over the sea. Altostratus clouds covered the warm sector. Low-level stratiform clouds over the sea can be seen to the west of the system.

The surface pressure, wind, and temperature time series as recorded at Tuktoyaktuk are shown in Fig. 16. The minimum surface pressure of 1012 hPa was recorded at 1700 UTC 30 September. A characteristic of the storm track disturbances was that the minimum pressures associated with them was higher than that associated with Pacific origin disturbances. The pressure trace is asymmetric with a relatively sudden reduction in pressure and relatively slow recovery. The winds at Tuktoyaktuk were from the south from 0600 to 1700 UTC on the 17th. By 0000 UTC on the 1st, they had shifted to northwesterly and remained from that direction for the duration of the event. The wind speeds increased in an approximate linear fashion throughout the event reaching a maximum value of 11 m s^{-1} by 1500 UTC on the 1st. The temperature record shows that there was an increase from −4.5°C at 1000 UTC to 0.4°C at 2200 UTC on the 30th. This was followed by a rapid decrease in temperature of approximately 2°C

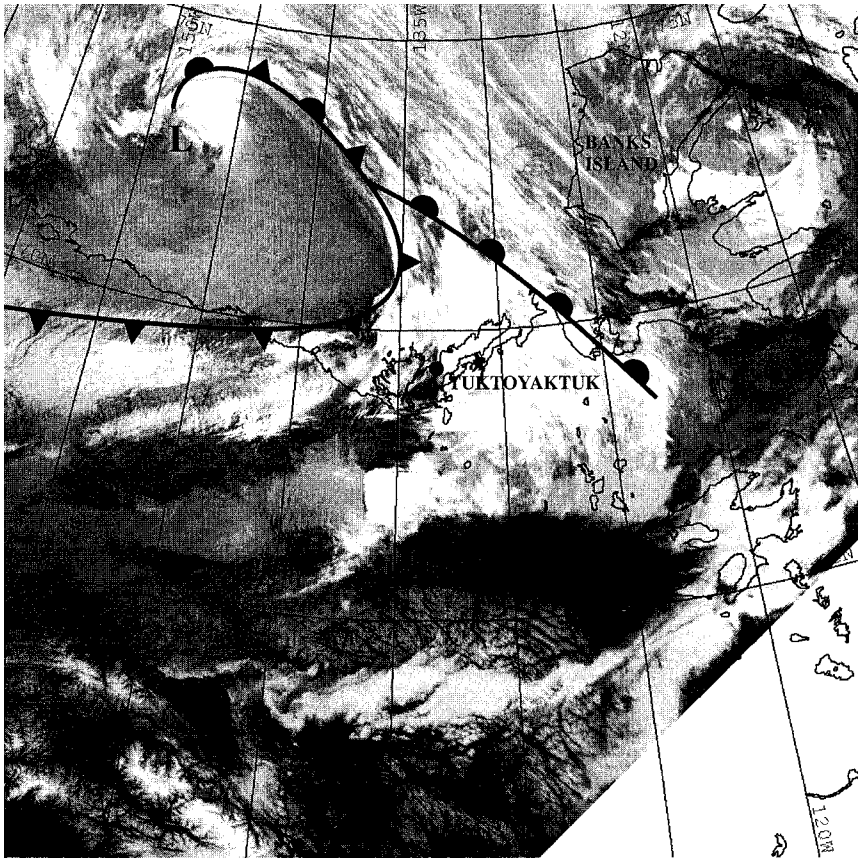

FIG. 15. Same as Fig. 4 but at 1901 UTC 30 September 1994 and the location of the vortex center labeled L.

between 2300 UTC on the 30th to 0300 UTC on the 1st and then a more gradual decrease during the rest of the event. This behavior of the surface data suggests that the warm front passed Tuktoyaktuk around 1800 UTC on the 30th with the cold frontal passage occurring approximately 6 h later. These times are consistent with the synoptic analyses discussed above.

The Tuktoyaktuk upper-air soundings at 0300 and 0600 UTC on the 1st are shown in Fig. 17. The 0300 UTC sounding shows a saturated layer below 1.8 km MSL associated with a uniform wind of 10 m s^{-1} out of the northwest. Between 1.8 and 3.5 km MSL, there was a humid but not saturated layer. In this layer, the wind speed was increasing with height while the wind direction was changing from southwesterly to westerly. A dry and relatively warm layer was present above 4.3 km that was associated with strong westerly winds. By 0600 UTC, there had seen a noticeable drying in the lower layer. The wind speed and direction in this layer were unchanged. There were also no significant changes in the other two layers with the exception of a slight descent, from 4.3 to 4.2 km MSL, in the temperature kink associated with the upper layer. This descent is thought to be associated with upper-tropospheric subsidence behind the synoptic-scale trough.

b. Radar observations

The radar reflectivity, horizontal wind, and divergence as observed at Tuktoyaktuk are shown in Fig. 18. Radar echoes were so weak in this case that radar reflectivity stronger than 11 dB*Z* were taken for analyses. Three distinct precipitation events can be seen in the data. There were two short and weak events around 1500 and 2000 UTC on the 30th. There was also a more significant and longer event between 0100 and 0400 UTC on the 1st. From the data previously presented, it is clear that the two weak events were associated with the passage of the warm front, while the more significant event was associated with the passage of the cold front. PPI radar echoes associated with the warm and cold front are shown in Figs. 19 and 21, respectively. Vertical profiles of reflectivity and wind field calculated from 10° PPI data are shown in Figs. 20 and 22. Weak echoes and relatively uniform west-northwesterly winds were observed during the warm front passage (Figs. 19 and

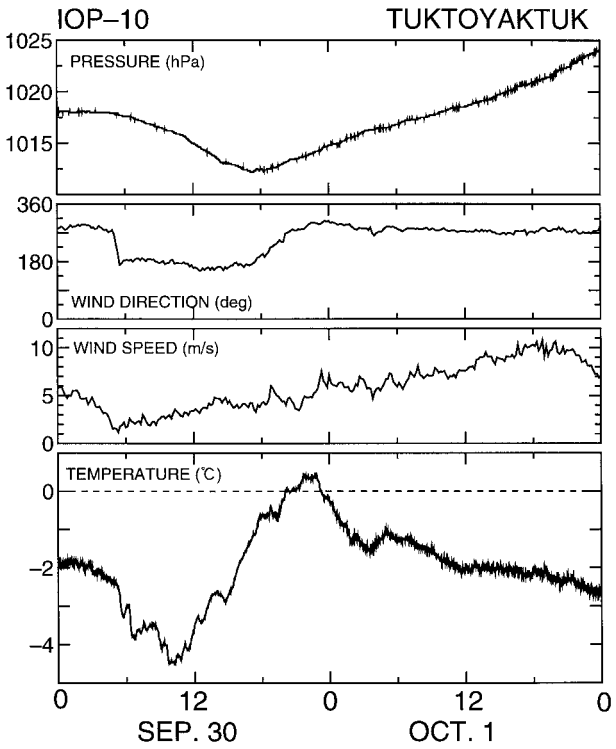

FIG. 16. Same as Fig. 5 but for IOP-10.

20). On the other hand, a band echo, which was oriented from southwest to northeast, with stronger reflectivity over 21 dBZ was approaching from the northwest (Fig. 21). Two peak winds were analyzed in the vertical profile (Fig. 22). One is the low-level northwesterly with a magnitude of 14 m s^{-1} at 0.8 km MSL. This direction corresponded to the movement of the band echo and it transported moisture from the Beaufort Sea. Another one is the upper-level southwesterly at 2 km MSL. This direction is almost corresponding to the band echo orientation. This echo passed over the radar site at 0150 UTC. Figure 18b shows that the wind field during the warm frontal events had relatively weak convergence that is consistent with the stratiform clouds that were associated with the warm front. In contrast, there was significant convergence associated with the cold frontal event that suggests that this event was convective in origin. This is supported by the satellite imagery shown in Fig. 15.

c. Moisture transport

The moisture transport, as diagnosed from the GANAL analysis, at the surface and 700 hPa at 1200 UTC on the 30th and 0000 UTC on the 1st are shown in Fig. 23. Also shown are the mean sea level pressure and the 700-hPa geopotential fields. From the figure, one can see the synoptic-scale low that was present southwest of the Aleutian Islands near 45°N, 170°W. The low was too far away to influence the transport in the area of interest. As a result, no moisture from the Pacific was associated with this event. In the vicinity of Tuktoyaktuk, one can clearly see the low-level transport of moisture associated with the disturbance under investigation. The source of this moisture is presumably the open waters of the Bering and Beaufort Seas. This transport is relatively shallow as it cannot be identified on the 700-hPa surface. The surface moisture transport also shows evidence of the frontal systems described earlier. In addition, at 700 hPa one can see evidence of the drying that was occurring at upper levels as the cold front passed Tuktoyaktuk.

6. Discussion

Based on all the data presented in this paper, conceptual models for the two classes of weather system discussed are shown in Fig. 24. Included are pathways

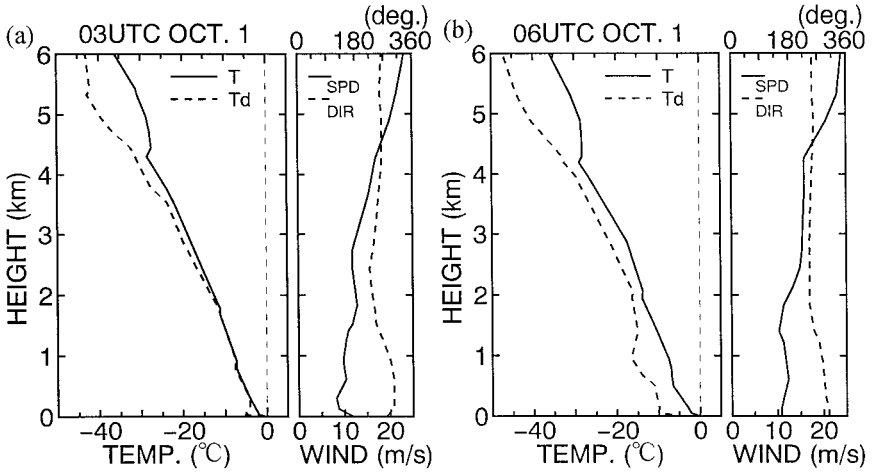

FIG. 17. Same as Fig. 6 but (a) 0300 and (b) 0600 UTC 1 October 1994.

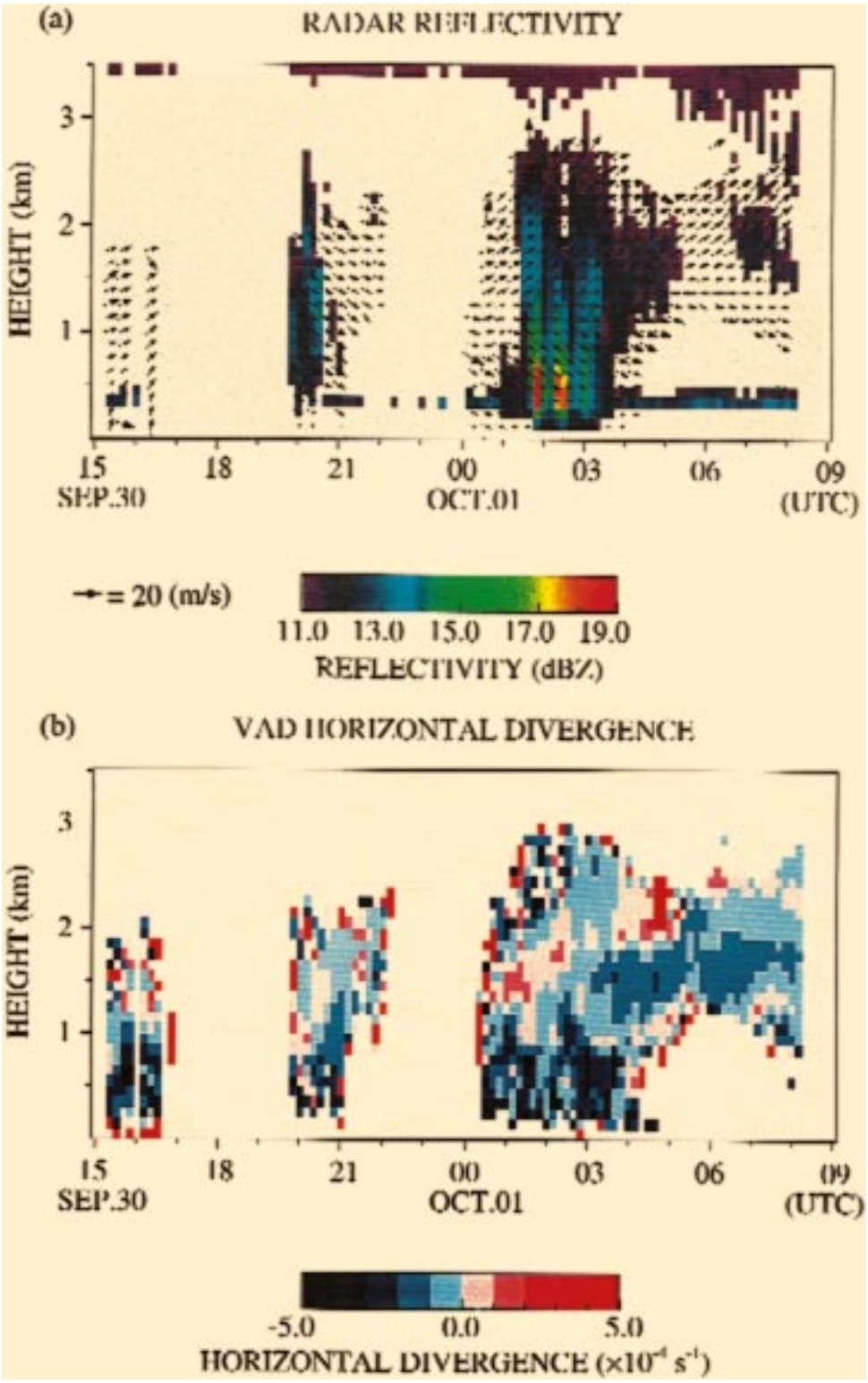

FIG. 18. Same as Fig. 7 but for IOP-10.

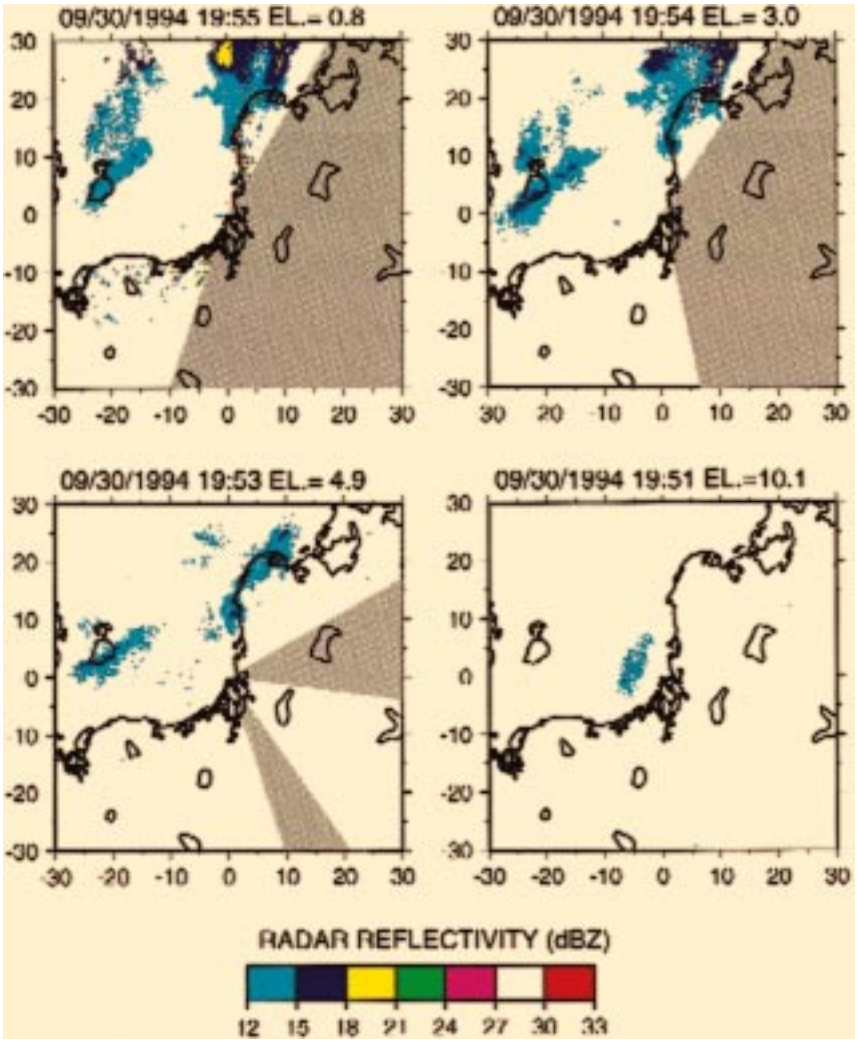

FIG. 19. Same as Fig. 8 but associated with warm front.

of the moist and dry airstreams associated with these systems.

Pacific origin disturbances occur when stationary, deep lows exist over the Gulf of Alaska and the northern Beaufort Sea. The location and intensity of these systems determine the upper-level circulation in the Tuktoyaktuk region. In particular, moisture from the Pacific is brought into the region by the low in the Gulf of Alaska. The movement of this system and the low-level moisture transport associated with it is blocked by the mountains along the west coast of the continent. The upper-level circulation associated with the system is unimpeded and its passage into the region of interest results in a lee cyclogenesis event. The secondary system that develops is relatively shallow. Its movement to the east and its interaction with the stationary Arctic front result in its intensification. This system controls the circulation in the lower layer. The presence of the two distinct circulation patterns at the surface and upper-level result in the distinct layering that was observed over the Tuktoyaktuk region. The layering associated with the disturbance had a larger impact on the precipitation that fell at Tuktoyaktuk. In the upper level, one observed weak precipitation that was organized on the mesoscale. The precipitation was intermittent in character. When the secondary depression was to the west of Tuktoyaktuk, the circulation associated with it brought dry continental air into the region. As a result, the precipitation produced aloft evaporated as it fell and did not reach the surface. As the depression passed Tuktoyaktuk, there was a shift in wind direction that brought moist air from the Beaufort Sea into the Tuktoyaktuk region. In this environment, the precipitation produced aloft was enhanced by the collection of cloud droplets and the coagulation of ice crystals. As a result, there was a significant accumulation of precipitation at the surface. The structure and evolution of the precipitation associated with this disturbance is similar to the ''seeder and feeder'' mechanism discussed by Hobbs (1978).

The structure and evolution of the storm track dis-

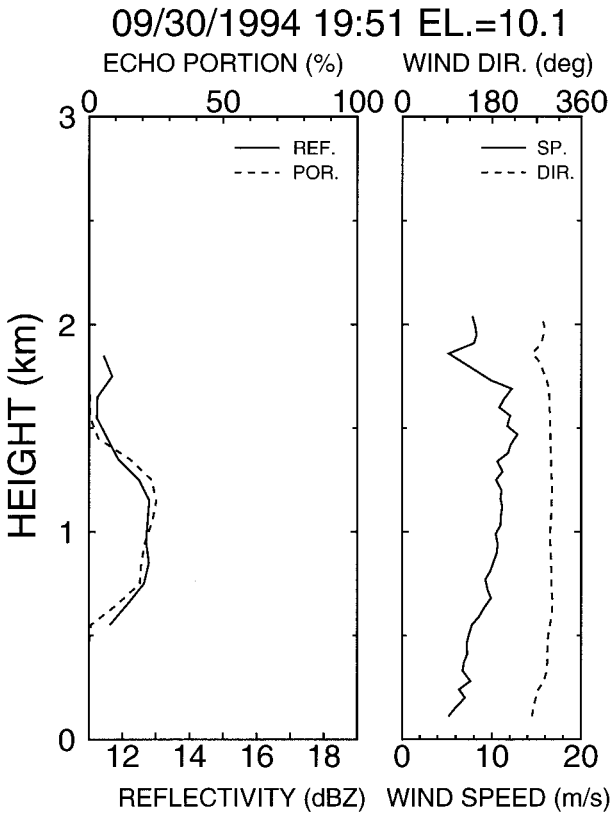

FIG. 20. Same as Fig. 9 but for 1951 UTC 30 September.

turbance was very different. This disturbance originated and propagated along the shallow baroclinic zone that developed along the ice edge. In addition, no upper-level moisture of Pacific origin was present. The disturbance that developed along the ice edge had warm and cold fronts associated with it. The precipitation that fell at Tuktoyaktuk was strongly modulated by the presence of the fronts. In particular, weaker stratiform precipitation was associated with the passage of the warm front, whereas the more intense convective precipitation, which was organized as a band structure, was associated with the passage of the cold front. In both instances, the source of the moisture was the Beaufort and Bering Seas. In addition, the descending dry air behind the cold front resulted in a drying of the upper level as the disturbance propagated eastward.

Ryan (1996) reviewed the conceptual models that have been developed for cyclonic systems and stressed the importance of these models for understanding the global water and energy cycles. The concept of the ''conveyor belt'' was first introduced for the analysis of the disturbances near the United Kingdom by Harrold (1973). He identified the conveyor belt as the moist air stream that ascends over the warm frontal zone from a region in advance of the surface cold front. Carlson (1980) applied these concepts to developing midlatitude cyclone over the United States. Browning and Monk (1982) and Browning (1990) generalized these ideas to extratropical cyclones. There are three major airstreams in their conceptual model. The ''warm conveyor belt'' (WCB) transported air from the southwest to the northeast ahead of the cold front; the ''cold conveyor belt'' (CCB) extended from the southeast to the northwest associated with the warm front. In addition, dry air was descending from the upper troposphere behind the cold front (the ''dry intrusion''). The WCB was ascending from the lower level along with the cold front and running over the CCB.

These disturbances are strongly affected by the geographic features, such as, land and sea extensions, coastlines, mountains, and sea ice extensions, etc. As a result, the conceptual models should be modified place to place. Hobbs et al. (1990, 1994) and Wang et al. (1994) suggested a conceptual model for weather systems over the central United States on the lee side of the Rocky Mountains. They reported the low pressure system associated with the dry trough and the Arctic front. The air mass advected to the northeast crossing from the Rocky Mountains had relatively dry and low equivalent potential temperature and it made the dry trough. The wet air mass from the Gulf of Mexico had high equivalent potential temperature and moved to the north. The pre–dry trough rainband formed at the confluence of both air masses due to the potential instability. When the cold air advection associated with the upper baroclinic zone encountered the warm air advection associated with the dry trough, the cold front aloft produced the ''cold frontogenesis aloft'' rainband in the east of the surface pressure trough. Weather systems are highly related with the geographic features.

Ryan and Wilson (1985) and Ryan et al. (1989) also reported on summertime frontal structure in southeastern Australia. The main air mass originally came from the midtroposphere over the Tasmanian Sea. It gradually subsided to reach the boundary layer over central Australia before turning southward and then ascending ahead of and over the surface front. Because the air mass came from the boundary layer in central Australia, it was drier and the cloud bases were higher. Significant evaporation occurred in the subcloud layer and it played an important role for the organization of mesoscale convections and the maintenance of the cold front. They regarded that this ascending airstream from central Australia was corresponding to the WCB in the Northern Hemisphere.

Considering the concept of the conveyor belt, the airstream from the Pacific Ocean in the Pacific origin disturbance, as illustrated in Fig. 24a, corresponds to the WCB. It supplies the warm and moist air mass from the Pacific Ocean to the Arctic region through the layer between 2 km and 3 km MSL. The ''generating cells'' were organized in this layer. Although the CCB was not clearly identified, another important moisture stream was coming from the Beaufort Sea in the lower layer

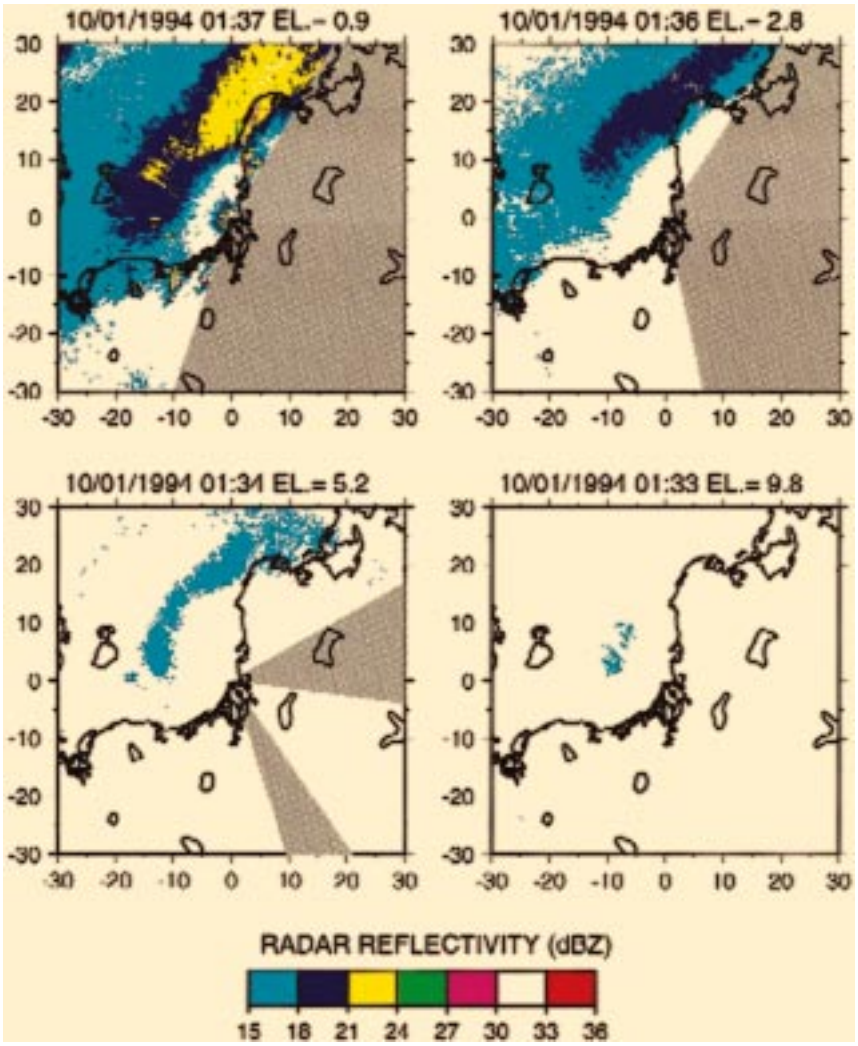

FIG. 21. Same as Fig. 8 but associated with cold front.

westward of the shallow depression, the precipitation was enhanced in this wet layer by means of the ''seeder and feeder'' mechanism. Although there are some similarities with systems in other parts of the world, the structure and evolution of the Pacific origin disturbance has, to the authors' knowledge, never been described before. On the other hand, the storm track disturbance had a very similar structure to that in the United States (Carlson 1980) and near the United Kingdom (Browning and Monk 1982; Browning 1990) as illustrated in Fig. 24b. The three conveyor belts (airstreams) may be seen in the satellite images and the objective data analyses. The WCB was identified ahead of the cold front coming from the Bering Sea. The CCB was identified eastward of the low in the lower layer. The WCB was in the lower altitude in the west part, that is, over Alaska and the Yukon and gradually ascending to the east to run over the CCB. The dry intrusion was also identified in the higher altitude (700- and 500-hPa charts). It made the moisture decrease west of the front near the center of the low and caused the vapor gradient in the west edge of the front to steepen. Other moisture was supplied to the WCB in the lower boundary layer from the open water over the Beaufort Sea. These features of the conveyor belt resemble the extratropical cyclone observed in the United States and near the United Kingdom as mentioned before.

7. Conclusions

The X-band Doppler radar observations were carried out at Tuktoyaktuk, Northwest Territories, Canada, during the fall of 1994 as part of BASE. The disturbances that were observed were classified into four main classes according to the scheme described in Hudak et al. (1995). Most of the systems fell into the categories of Pacific origin or storm track disturbance. In this paper, the structure and evolution of a representative system

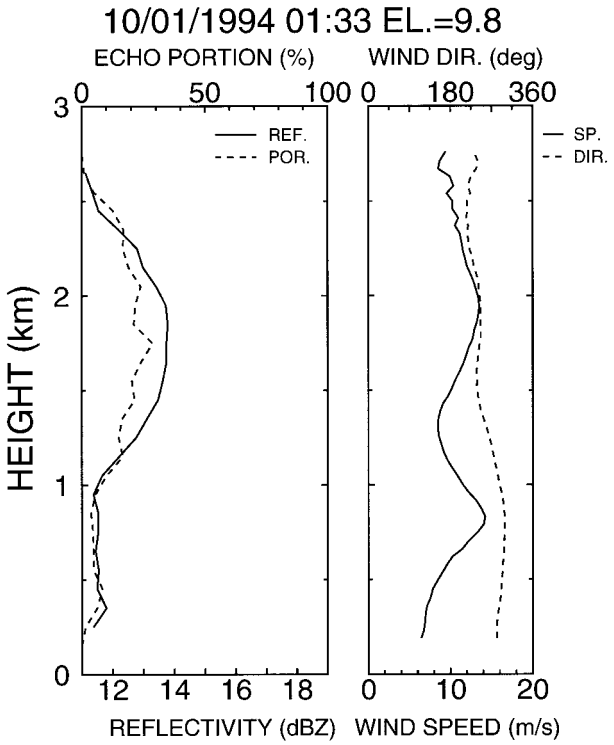

FIG. 22. Same as Fig. 9 but for 0133 UTC 1 October.

from each of these categories has been described. A conceptual model based on the observations described in this paper for each of these types of storms is shown in Fig. 24.

The evolution of the Pacific origin disturbances appears to be as follows. Stationary synoptic-scale systems are present over the Gulf of Alaska and the northern Beaufort Sea. The interaction of the Gulf of Alaska low with the mountains along the west coast of North America results in the development of a secondary lee cyclone. This system interacts with a stationary Arctic front as it moves eastward. In the Tuktoyaktuk region, the presence of these systems results in a distinct two-layer structure. In the upper layer, southerly airflow brings moisture from the Gulf of Alaska system into the region. Weak precipitation organized by mesoscale generating cells was observed in this layer. The characteristics of the low-level air mass was controlled by the secondary depression. When it was located to the west of Tuktoyaktuk, the circulation associated with it brought dry continental air into the region. As a result, the precipitation produced aloft evaporated before it reached the ground. As the depression moved eastward, the concomitant change in wind direction brought moist air from the Beaufort Sea into the region. The precipitation produced aloft was now enhanced in a sort of seeder–feeder mechanism.

The storm track disturbance was associated with the passage of a small but intense mesoscale cyclone along the ice edge in the Beaufort Sea. No strong synoptic-scale forcing was present in the Gulf of Alaska and moisture from the Pacific did not influence the system. The cyclone had well-developed warm and cold fronts associated with it. The precipitation associated with the system was strongly organized by the presence of these fronts. Although of smaller horizontal extent than typical midlatitude cyclones, its structure and evolution were nevertheless similar. In particular, the three airstreams—the WCB, the CCB, and the dry intrusion—identified by Browning and Monk (1982) and Browning (1990) as occurring in cyclones near the British Isles can be identified in this high-latitude system. The source of moisture for this system came from the Beaufort and Bering Seas.

This is the first report to describe weather systems observed during BASE. Further detailed analyses by means of synoptic data, objectively analyzed fields, upper-air soundings, satellite data, and numerical model simulations will be needed before a complete picture of the weather systems in the area and their contribution to the water and energy cycles is forthcoming.

Acknowledgments. The authors would like to express their thanks to Ronald E. Stewart, David R. Hudak, and Edward T. Hudson, Atmospheric Environment Service, Canada, and Hiroshi Uyeda, Hokkaido University, for their encouragement of field studies and analyses. They also express their thanks to Taisuke Shimamura, Hokkaido University; Michael Crowe and Ray Beaubien, Atmospheric Environment Service, Canada; and Sgt. R. P. Near, Royal Canadian Mounted Police, Canada, for their assistance in the radar observations at Tuktoyaktuk, Northwest Territories, Canada.

A part of this project was supported by ''Grant-in-Aid for International Scientific Research'' of the Ministry of Education, Science, Sports and Culture (Monbusyo), Japan.

REFERENCES

Aggaard, K., and E. C. Carmack, 1989: The role of sea ice and other fresh waters in the Arctic circulation. *J. Geophys. Res.,* **94,** 14 485–14 998.

Barry, R. G., M. C. Serreze, J. A. Maslanik, and R. H. Preller, 1993: The Arctic sea ice-climate system: Observations and modeling. *Rev. Geophys.,* **31,** 397–422.

Browning, K. A., 1990: Organization of clouds and precipitation in extratropical cyclones. *Extratropical Cyclones: The Erik Palmén Memorial Volume,* C. W. Newton and E. O. Holopainen, Eds., Amer. Meteor. Soc., 129–153.

——, and R. Wexler, 1968: The determination of kinetic properties of a wind field using Doppler radar. *J. Appl. Meteor.,* **7,** 105–113.

——, and G. A. Monk, 1982: A simple model for the synoptic analysis of cold fronts. *Quart. J. Roy. Meteor. Soc.,* **108,** 435–452.

Carlson, T. N., 1980: Airflow through midlatitude cyclones and the comma cloud pattern. *Mon. Wea. Rev.,* **108,** 1498–1509.

Cattle, H., 1985: Diverting Soviet rivers: Some possible repercussions for the Arctic Ocean. *Polar Rec.,* **22,** 485–498.

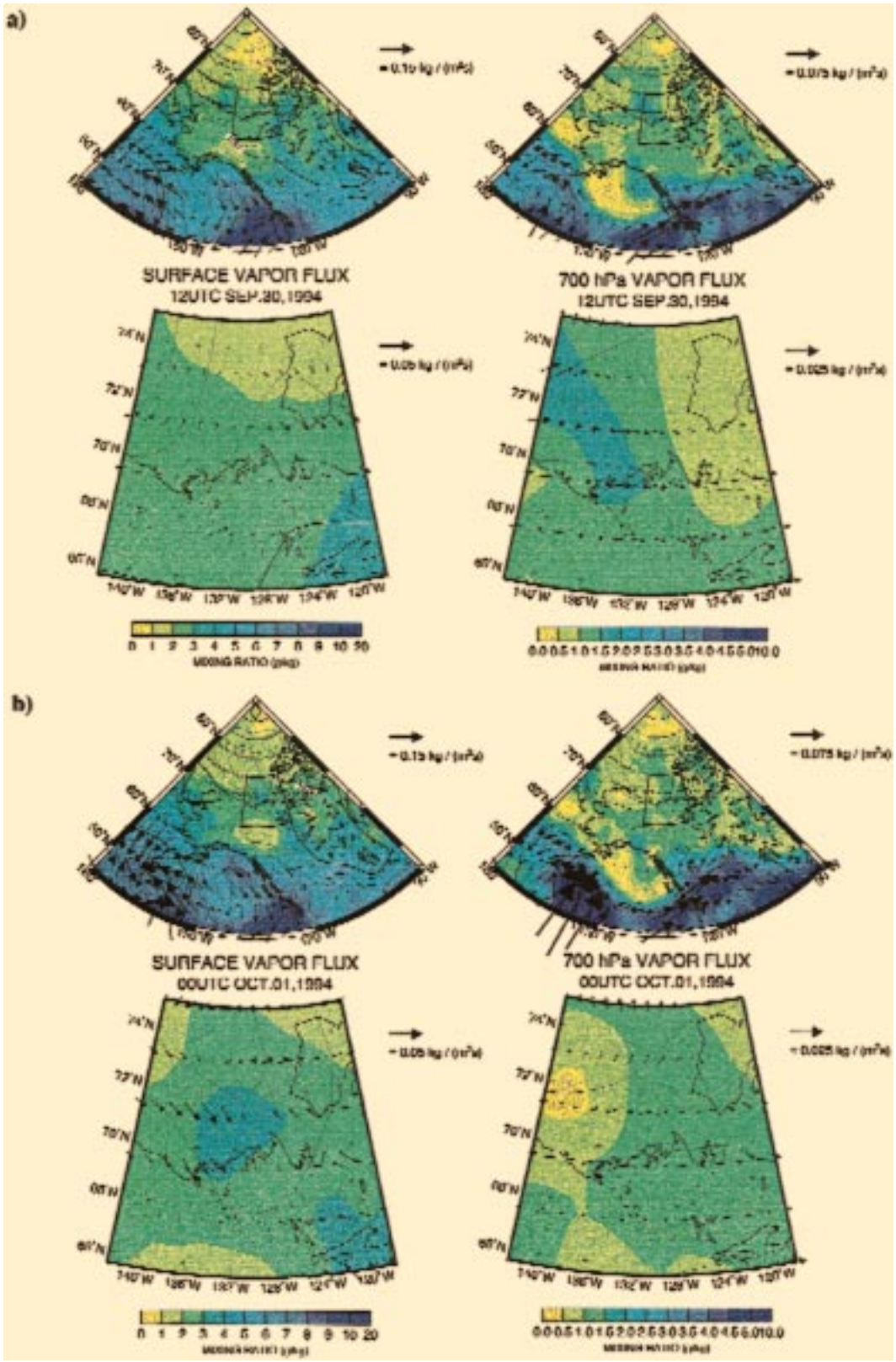

FIG. 23. Same as Fig. 13 but for (a) 1200 UTC 30 September and (b) 0000 UTC 1 October 1994.

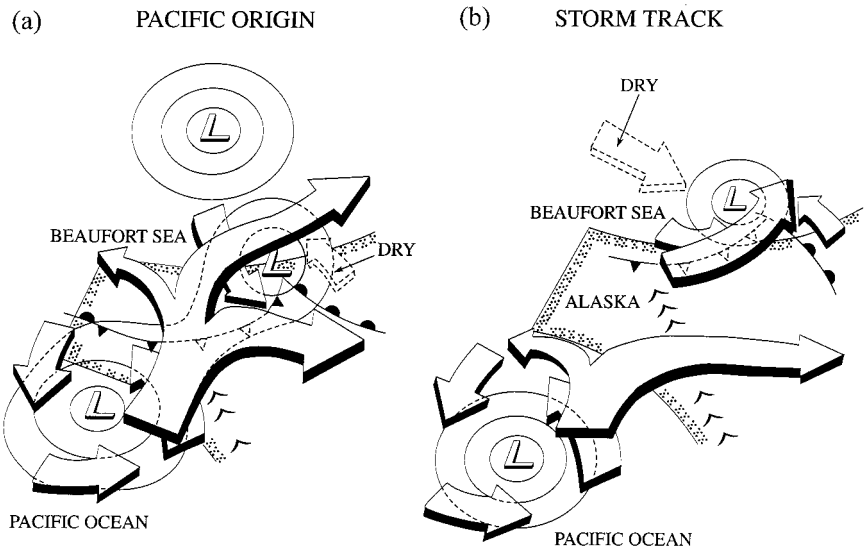

FIG. 24. Conceptual models for (a) Pacific origin and (b) storm track disturbances. Simplified synoptic conditions and topography around the BASE experimental region were shown in the figure. Solid and wide arrows indicate wet airstreams and dashed arrows indicate dry airstreams.

Chanine, M., 1992: The hydrological cycle and its influence on climate. *Nature,* **359,** 373–380.

Fujiyoshi, Y., T. Takeda, and K. Kikuchi, 1982: Observation of wintertime clouds and precipitation in the Arctic Canada (POLEX-North). Part III: Radar observation of precipitating clouds. *J. Meteor. Soc. Japan,* **60,** 1227–1237.

Gunn, K. L. S., M. P. Langleben, A. S. Dennis, and B. A. Power, 1954: Radar evidence of a generating level for snow. *J. Meteor.*, **11,** 20–26.

Harrold, T. W., 1973: Mechanisms influencing the distribution within baroclinic disturbances. *Quart. J. Roy. Meteor. Soc.,* **99,** 232–251.

Higuchi, K., T. Takeda, and K. Kikuchi, Eds., 1981: Observations of clouds and precipitation in the Arctic Canada. Final Rep. on the Monbusyo International Scientific Research, Nagoya University, Nagoya, Japan, 189 pp.

Hobbs, P. V., 1978: Organization and structure of clouds and precipitation on the mesoscale and microscale in cyclonic storms. *Rev. Geophys. Space Phys.,* **16,** 741–755.

——, J. D. Locatelli, and J. E. Martin, 1990: Cold fronts aloft and the forecasting of precipitation and severe weather east of the Rocky Mountains. *Wea. Forecasting,* **5,** 613–626.

——, ——, and ——, 1994: A new conceptual model for topographically altered cyclones in the central United States. Preprints, *Sixth Conf. on Mesoscale Processes,* Portland, OR, Amer. Meteor. Soc., 213–214.

Hudak, D. R., R. E. Stewart, G. W. K. Moore, and E. T. Hudson, 1995: Synoptic considerations of storms in the southern Beaufort Sea—Expectations for BASE. Preprints, *Fourth Conf. on Polar Meteorology and Oceanography.* Dallas, TX, Amer. Meteor. Soc., 234–237.

Kikuchi, K., 1970: Peculiar shapes of solid precipitation observed at Syowa Station, Antarctica. *J. Meteor. Soc. Japan,* **48,** 243–249.

——, Ed., 1987: Studies on the snow crystals of low temperature types and Arctic aerosols. Final Rep. on the Monbusyo International Scientific Research, Hokkaido University, Sapporo, Japan, 283 pp.

——, and M. Kajikawa, 1979: Comments on V-shaped snow crystals observed in Arctic Canada. *J. Meteor. Soc. Japan,* **57,** 484–487.

——, S. Tsuboya, N. Sato, Y. Asuma, T. Takeda, and Y. Fujiyoshi, 1982: Observation of wintertime clouds and precipitation in the Arctic Canada (POLEX-North). Part II: Characteristic properties of precipitation particles. *J. Meteor. Soc. Japan,* **60,** 1215–1226.

Magono, C., Ed., 1978: Snow crystals in the Arctic Canada. Final Rep. on the Monbusyo International Scientific Research, Hokkaido University, Sapporo, Japan, 172 pp.

——, and K. Kikuchi, 1980: Some observation of snowfall and meteorological conditions in Arctic Canada. *Mon. Wea. Rev.,* **108,** 1656–1664.

Renfrew, I. A., and G. W. K. Moore, 1996: Mesoscale cyclones in the Canadian Arctic. Preprints, *Seventh Conf. on Mesoscale Processes,* Reading, United Kingdom, Amer. Meteor. Soc., 95–97.

Ryan, B. F., 1996: On the global variation of precipitating layer clouds. *Bull. Amer. Meteor. Soc.,* **77,** 53–70.

——, and K. J. Wilson, 1985: The Australian summertime cool change. Part III: Subsynoptic and mesoscale model. *Mon. Wea. Rev.,* **113,** 224–240.

——, ——, and E. J. Zipser, 1989: Modification of the thermodynamic structure of the lower troposphere by the evaporation of precipitation ahead of a cold front. *Mon. Wea. Rev.,* **117,** 138–153.

Takeda, T., Y. Fujiyoshi, and K. Kikuchi, 1982: Observation of wintertime clouds and precipitation in the Arctic Canada (POLEX-North). Part I: Characteristic features of clouds and precipitation. *J. Meteor. Soc. Japan,* **60,** 1203–1214.

Wang, P.-Y., J. E. Martin, J. D. Locatelli, and P. V. Hobbs, 1994: Recurrent precipitation bands within winter cyclones in the central United States. Preprints, *Sixth Conf. on Mesoscale Processes,* Portland, OR, Amer. Meteor. Soc., 215–217.